Synthesis, Crystal Structure, Spectroscopy, and Theoretical Investigations of Tetrahedrally Distorted Copper(II) Chelates with $[CuN_2S_2]$ Coordination Sphere

Stephan Knoblauch,[a] Roland Benedix,[b] Martin Ecke,[a] Thomas Gelbrich,[c] Joachim Sieler,[a] Fernando Somoza,[a] and Horst Hennig*[a]

Keywords: Copper chelates / EPR spectroscopy / Electronic structure / Schiff base ligands / Structure elucidation

A series of tetrahedrally distorted copper(II) complexes with thiolate and imine coordination were synthesized. Schiff bases derived from 4-benzoyl-3-methyl-1-phenyl-2-pyrazoline-5-thione and various diamines were used as tetradentate ligands to obtain tetrahedrally distorted metal chelates with $[CuN_2S_2]$ complex units. Crystal structures of the complexes **1**, **2**, **5** and **6** and of ligand H_2**5** have been determined by means of single-crystal X-ray structure analysis. The structure data show a strong influence of the diamine building blocks on the tetrahedral distortion of the copper(II) complexes. Results of Extended Hückel LCAO calculations correlate strongly with structural, electrochemical, UV/Vis- and EPR-spectroscopic features obtained experimentally. The calculations confirm for the whole complex series a strong delocalization of the frontier orbitals. The highest fully occupied molecular orbital shows a weak contribution, resulting from thiolate donor atoms, whereas the antibonding singly occupied molecular orbitals (SOMOs) are distributed between the copper(II) centre (ca. 35–40%) and the N_2S_2 donor set. The SOMO energy significantly lowers with increasing tetrahedral distortion of the coordination sphere. The influence of the tetrahedral distortion of copper(II) complexes on redox potentials, UV/Vis and EPR spectra is discussed.

Introduction

Numerous examples of copper coordination in the active sites of proteins are known.[1][2] These highly specialized molecules fulfil special requirements to manage electron and dioxygen transfer.[3][4] Particularly the Cu^I/Cu^{II} redox couple is a matter of importance.[5] Since the elucidation of crystal structures of plastocyanin (e.g. *Populus nigra*[6]) and azurin (e.g. *Pseudomonas aeruginosa*[7]), much attention is focused on modelling these *Type I* copper active sites,[8][9] also with respect to their unusual spectroscopic and electronic properties.[10][11] Moreover, the Cu_A electron transfer site in *cytochrome c oxidase* contains copper thiolate bonds.[12] With respect to the biomimetic modelling of these active sites, the chemistry of copper complexes with simultaneous imine and thiolate coordination has expanded during the last two decades.

The uncommon electron transfer properties of copper(II) ions in a low-symmetry environment of imino and thiolato donor sets led us to photochemical studies of various copper(II) chelates of $[CuN_2S_2]$ constitution.[13] It could be shown, that $[CuN_2S_2]$ chelates with Schiff base ligands derived from appropriate pyrazoline-5-thiones lead to unusual photo-induced electron transfer reactions, when irradiated in the presence of (porphyrin)metal(III) compounds and cycloolefins like α-pinene.[14–16] However, the role of the $[CuN_2S_2]$ complexes in these coupled electron transfer processes could not be sufficiently explained.

The $[CuN_2S_2]$ complexes **1**–**4**, **7**, and **9** and the corresponding ligands (H_2**1**–H_2**4**, H_2**7**, and H_2**9**) were synthesized for the first time whereas **5**, **6**, and **8** are already known from the literature.[17][18] The complex series **1**–**9** belong to the relatively few examples of stable copper(II) complexes with thiolate coordination[19] and are characterized by UV/Vis-spectroscopic similarity to Blue copper proteins.[20–23] The Schiff base ligands (see Figure 1) were obtained by condensation of 4-benzoyl-3-methyl-1-phenyl-2-pyrazoline-5-thione with selected diamines as proposed by Toftlund.[17] The choice of the bridging diamines was planned with the aim to control the geometry around the copper centre. Parallel with the structural changes of the Schiff base ligands a change in the spectral features of the corresponding Cu^{II} complexes occurs.[24][25] However, the UV/Vis spectra of that kind of copper(II) Schiff base complexes featuring large π-systems are not very well understood. EHT-LCAO calculations were carried out, therefore, as an approach to better understand the spectroscopic as well as electronic properties of these compounds. The calculations are based on crystal-structure data obtained for complexes **1**, **2**, **5**, and **6**. Crystal-structure data of the 2,2′-biphenylene-bridged compound **8** were taken from the literature.[17]

The goal of this study is to find the geometrical parameters introduced by the different ligand backbones which govern the deformations of the usually preferred planar coordination sphere for copper(II) ions in $[CuN_2S_2]$ chelates. An attempt is made to correlate EHMO data with UV/Vis-

[a] Institut für Anorganische Chemie der Universität Leipzig, Talstraße 35, D-04103 Leipzig, Germany
Fax: (internat.) +49(0)341/9604600
E-mail: hennigho@sonne.tachemie.uni-leipzig.de
[b] Bereich Naturwissenschaften der HWTK Leipzig, Postfach 66, D-04251 Leipzig, Germany
[c] University of Southampton, Department of Chemistry, Highfield, Southampton SO17 1BJ, United Kingdom

  1434–1948/99/0808–1393 $ 17.50+.50/0

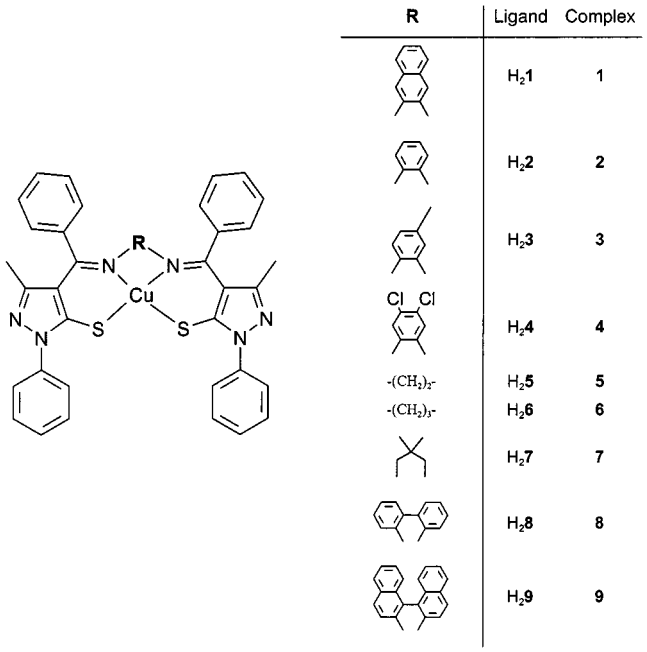

Figure 1. Formula scheme of copper(II) complexes **1**−**9**

and EPR-spectroscopic results as well as previously reported electrochemical parameters.[13]

Results and Discussion

Structures of the Schiff Base Ligand H_2**5** and of the Copper(II) Complexes 1, 2, 5, and 6

The crystal structure of the ligand H_2**5** has been determined to estimate the influence of the metal ion on the structural changes which occur upon deprotonation and coordination (see Figure 2 and Table 1).

Because no viable solution resulted perceiving $Z = 8$ and *C*2/*c*, space group *Cc* was applied yielding two independent molecules in the asymmetric unit. Figure 3 displays these molecules superimposed along the ethylenediamine fragments N(1)−C(35)−C(36)−N(2) and N(7)−C(71)−C(72)−N(8), respectively. This proves that the two molecules within the asymmetric unit are conformationally independent. Both molecules crystallize in the thioketone tautomeric form and show no symmetry. Considering the C(35)−C(36) [or C(71)−C(72)] axis, H_2**5** shows an antiperiplanar conformation which is changed to a gauche arrangement upon deprotonation and coordination of copper(II) ions. In addition, the ligand H_2**5** is characterized by two weak hydrogen bonds between the pyrazolinethione S atoms and the N atoms of the bridging ethylenediamine unit (Figure 2 and Table 2).

In agreement with available crystal-structure data of **8**,[17] none of the investigated complexes show two-fold symmetry. In general, neither **1**, **2**, **5**, nor **6** can be ordered to any symmetry element (C_1). The intermolecular distances between single molecules of **1**, **2**, **5**, and **6** in the corresponding crystal lattices refer to discrete monomeric species without any interactions. Crystal data of **1**, **2**, **5**, and **6** are listed in Table 1. Selected bond lengths and angles are given in Table 3 and perspective views are displayed in Figures 4, 5, and 6.

The copper(II) centre in all considered complexes is surrounded by a more or less flattened tetrahedron of two imine nitrogen atoms and two thiolate sulfur atoms. Figure 7 visualizes the most important geometrical parameters of the coordination spheres in **1**, **2**, **5**, **6**, and **8**. The deviation from the planar arrangement can be assessed in a first approach by means of the interplanar angles between the two planes defined by the atoms N(1)−Cu−S(1) and N(2)−Cu−S(2)

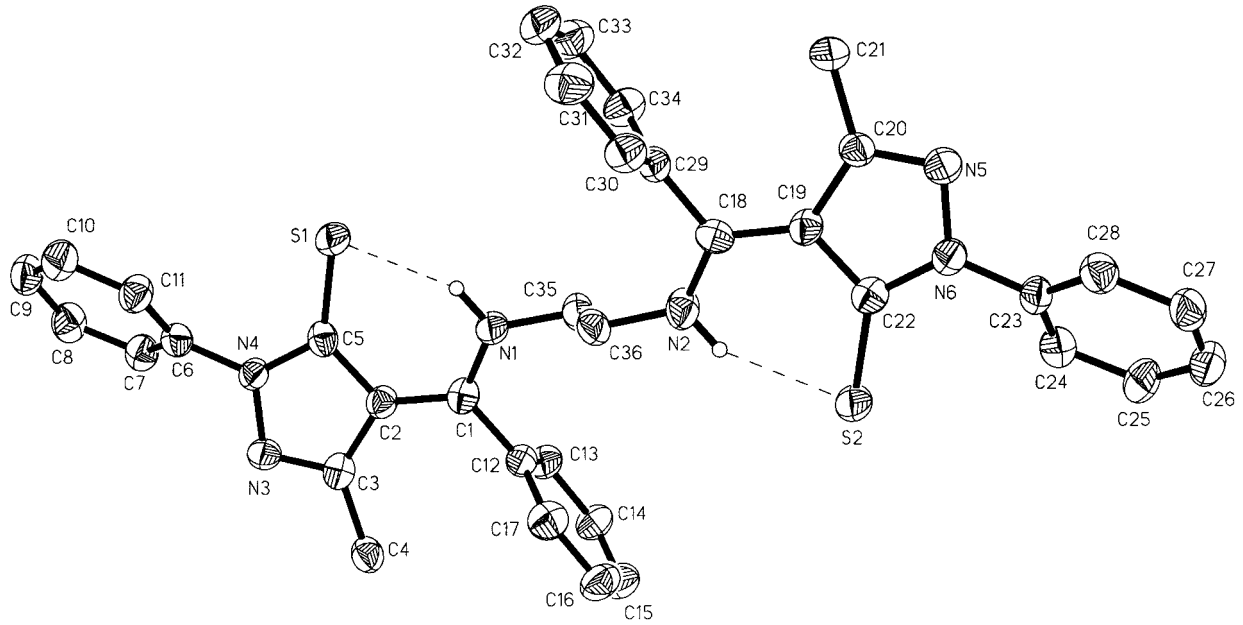

Figure 2. Molecular structure and numbering scheme of ligand H_2**5**; with exception of N(1)H and N(2)H hydrogen atoms are omitted for clarity (ORTEP drawing with 50% probability ellipsoids)

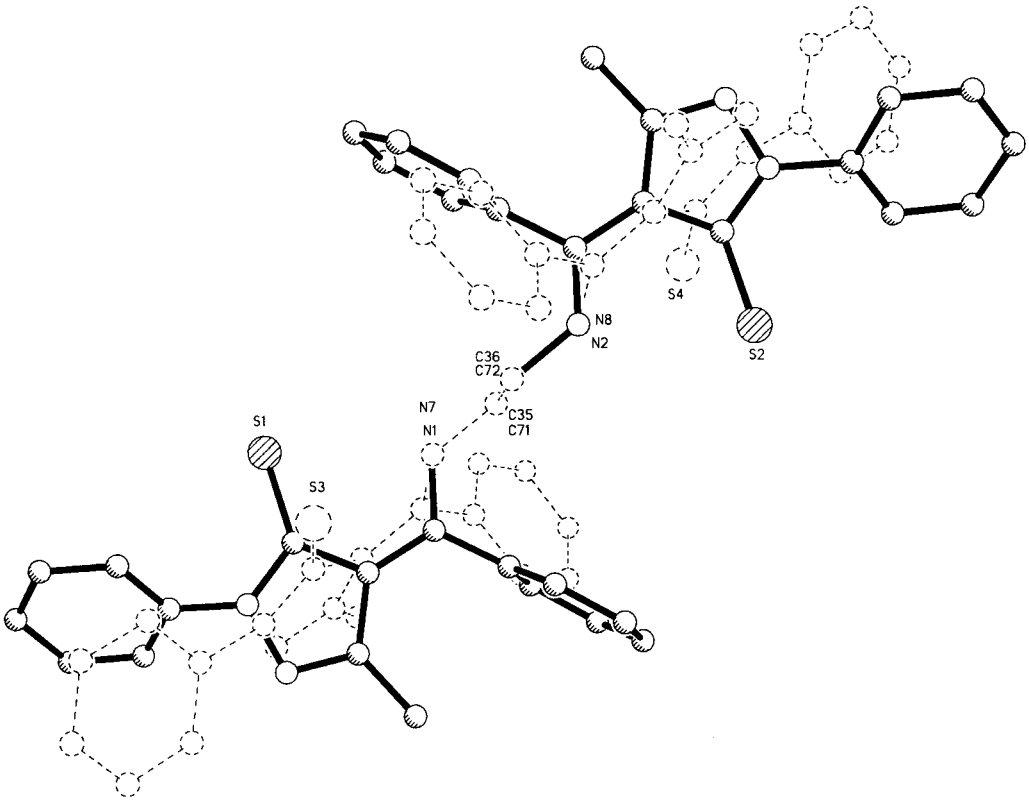

Figure 3. View of the two molecules of H_2**5** (solid lines and dashed lines, respectively) as present in the crystal; hydrogen atoms are omitted for clarity (ORTEP drawing with 50% probability ellipsoids)

Table 1. Crystallographic data and data related to data acquisition and refinement for compounds H_2**5**, **1**, **2**, **5,** and **6**

	H_2**5**	**1**	**2**	**5**	**6**
Empirical formula	$C_{36}H_{32}N_6S_2$	$C_{44}H_{32}CuN_6S_2$	$C_{40}H_{30}CuN_6S_2{\cdot}CHCl_3$	$C_{36}H_{30}CuN_6S_2{\cdot}H_2O$	$C_{37}H_{32}CuN_6S_2$
Molecular mass	612.81	772.42	841.72	692.32	687.35
Crystal size [mm]	0.25 × 0.12 × 0.10	0.40 × 0.20 × 0.20	0.26 × 0.20 × 0.20	0.50 × 0.20 × 0.20	0.30 × 0.24 × 0.24
Crystal system	monoclinic	monoclinic	monoclinic	orthorhombic	hexagonal
Space group	*Cc*	$P2_1/n$	$P2_1/n$	$Pna2_1$	$P6_1$
Unit cell dimensions					
a [Å]	12.143(1)	10.0339(7)	10.569(1)	13.050(3)	14.2559(6)
b [Å]	19.172(1)	26.005(2)	34.605(5)	10.550(2)	14.2559(6)
c [Å]	26.638(1)	16.054(1)	10.696(2)	23.990(5)	28.510(2)
α [°]	90	90	90	90	90
β [°]	94.10(1)	94.1520(10)	95.24(2)	90	90
γ [°]	90	90	90	90	120
V [Å^3]	6176.9(3)	4178.0(5)	3896(1)	3303(1)	5017.9(4)
Z	8	4	4	4	6
ρ(calcd.) [g/cm^3]	1.305	1.228	1.435	1.388	1.367
μ [mm^{-1}]	0.286	0.659	0.912	0.827	0.814
Absorption correction		SADABS	ψ scans	SADABS	SADABS
θ range for data collection	1.53° < θ < 26.00°	1.49° < θ < 26.14°	2.00° < θ < 25.98°	1.70° < θ < 26.28°	1.65° < θ < 26.23°
Reflections collected	44478	18221	7302	15133	22883
Independent reflections	12045	7272	5719	4789	6150
Final *R* indices [$I > 2\sigma(I)$]	$R = 0.0566$	$R = 0.0566$	$R = 0.0525$	$R = 0.0344$	$R = 0.0528$
	$wR_2 = 0.1330$	$wR_2 = 0.1427$	$wR_2 = 0.1051$	$wR_2 = 0.0685$	$wR_2 = 0.1329$
R indices (all data)	$R = 0.0830$	$R = 0.1181$	$R = 0.2285$	$R = 0.0464$	$R = 0.0718$
	$wR_2 = 0.1440$	$wR_2 = 0.1746$	$wR_2 = 0.1570$	$wR_2 = 0.0733$	$wR_2 = 0.1526$
Absolute structure parameter	0.07(6)	–	–	0.01(1)	0.02(2)

(θ), or by the sum (Σ) of each of the four angles N(1)−Cu−S(1), S(1)−Cu−S(2), S(2)−Cu−N(2), and N(2)−Cu−N(1) (Σ = 360° for an ideal planar arrangement and Σ = 437.6° for an ideal tetrahedral arrangement of all donor atoms in CuN_2S_2 units).

In complex **1**, the copper(II) ion is bound to the imine and thiolate donors in an essentially planar arrangement (see Figure 4). The copper ion in the crystal lattice of **1** deviates by 0.0413 Å from the calculated least-squares plane of the four donor atoms $N_{(1)}-N_{(2)}-S_{(1)}-S_{(2)}$. As expected,

Table 2. Bond lengths [Å] and bond angles [°] for hydrogen bonds in H_2**5**

D−H···A	*d*(D−H)	*d*(H···A)	*d*(D···A)	<(DHA)
N(1)−H(1)···S(1)	0.88	2.25	3.018(3)	145.3
N(2)−H(2)···S(2)	0.88	2.26	3.022(4)	145.3
N(7)−H(7A)···S(3)	0.88	2.32	3.039(4)	138.8
N(8)−H(8A)···S(4)	0.88	2.30	3.025(4)	140.2

θ increases in the order **1**, **2**, **5**, **6**, and **8** due to increasing steric demands of the different diamine backbones (Table 3). Depending on the amine bridge used, five- [**1**−**5**, Cu−N(1)−C(35)−C(36)−N(2)], six- [**6**−**7**, Cu−N(1)−C(35)−C(36)−C(37)−N(2)], or seven-membered chelate rings (**8**−**9**) form.

Even though complexes **1** and **5** both feature five-membered chelate rings, complex **1** with a bridging naphthyl unit shows distinct differences in θ values from the dihedral angle determined for complex **5**. This can be attributed to the different ligand flexibilities resulting from hindered rotation around the bond C(35)−C(36) in **1** or to larger conjugative effects of the aromatic bridging units forcing the system **1** into a planar donor arrangement to attain a more efficient π overlap.

In agreement with complexes containing comparably combined *N*,*S*-coordinating ligands,[26] a larger bite angle for the two N donors (N_1−Cu−N_2 in Figure 7) increases the tendency to form a pseudotetrahedral coordination sphere. This angle is influenced by both the steric demands of the corresponding backbone **R** connecting the N donors and the conformational flexibility of **R**. Consequently, a stronger distortion was observed for **6** [N(1)−Cu−N(2): 91.6°, θ = 42.5°] and **8** than for **1**, **2** and **5** due to the larger N(1)−Cu−N(2) bite angle.

A comparable Schiff base Cu^{II} complex synthesized by Gullotti consisting of 3-formyl-1-phenyl-2(1*H*)-pyridinethione and a propylene bridge shows a weaker effect on the coordination geometry (N−Cu−N′: 89.2°; N−Cu−N′/S−Cu-S′: 19.6°).[27] On the other hand, Bereman observed a particularly strong tetrahedral distortion of 53° for [*N*,*N*′-trimethylenebis(methyl 2-amino-1-cyclopentenedithiocarboxylato)]copper(II) (N−Cu−N′: 93.1°; N−Cu−N′/S−Cu−S′: 53°).[28] Steric influence of the different ligand frameworks and bonding behaviour of the coordinating sulfur donors may be responsible for the observed differences.

The geometry of the pyrazole units of the chelates **1**, **2**, **5**, and **6** shows no significant changes due to the influence of different backbones **R** (see Table 3). The pyrazole rings including the sulfur donors are almost planar in all cases and none of the atoms in the units S(1)−N(3)−N(4)−C(2)−C(3)−C(5) and S(2)−N(5)−N(6)−C(19)−C(20)−C(22), deviate more than 0.0618 Å [S(1) in **1**] from the least-squares planes defined by these atoms.

The sulfur−sulfur distances (3.13, 3.17, 3.08 Å) and S(1)−Cu−S(2) angles (88.3, 90.2, 87.3°) for **1**, **5**, **6**, respectively are also nearly uneffected by the different diamine bridges. This finding shows that, if in a first approximation the S_2Cu fragment remains almost unchanged, the geometrical changes forcing the system from planar to pseudotetrahedral donor arrangements are mainly a result of the different positions of the imine donors relative to the copper ion, and the different modes of coordination are obtained through simultaneous torsions along the bisector of the S_1−Cu−S_2 angle (Figure 7).

EHMO Calculations Related with UV/Vis, EPR, and Electrochemical Data

The UV/Vis spectra of H_2**1**−H_2**9** were used to estimate the spectral changes occurring upon deprotonation and coordination of the copper(II) ion. All ligands feature three intense bands in the region between 270 and 450 nm (Table 4). The two bands in the ultraviolet part of the spectrum are, in accordance to their intensities, attributable to π-π* transitions within the aromatic system and the azomethine or the thiolate chromophore, respectively. These absorptions appear at lower energies for the Schiff bases with aromatic coupling between the two imine groups via phenyl or biphenyl units (H_2**1**−H_2**4**, H_2**8**−H_2**9**), since the larger system of conjugated double bonds gives rise to a smaller energy gap between the highest occupied (HOMO) and the lowest unoccupied molecular orbitals (LUMO). The third absorption peaks in the visible region are less intense for H_2**1**−H_2**9**, but they can also be attributed to π-π* transitions since their intensities are too high for forbidden n-π* transitions. These bands disappear upon coordination of the metal ion.

To elucidate the electronic structure of copper complexes **1**−**9** in relation to their spectroscopic features, Extended Hückel MO calculations were performed. According to L. Hennig,[17] the UV/Vis spectra of the analogous complexes with hydrogen atoms instead of phenyl groups bound to the imine functions are nearly identically with those of **1**−**9**. This shows that electronic transitions are not significantly influenced by the phenyl groups on C(1) and C(18). In order to simplify molecules **1**−**9**, the smaller hydrogen-substituted systems were used as model fragments for the EHMO calculations, and the two hydrogen atoms were calculated in ideal positions.

Figure 8 displays the frontier orbital region of the fragment derived from the ethylene-bridged [CuN_2S_2] complex **5** belonging to the point group C_1. In agreement with previous MO calculations on copper dithiolates,[29][30] the highest singly occupied MO (SOMO) correlates with an antibonding orbital. It is formed by σ-type lone-pair orbitals of the ligand and a copper d orbital described as an admixture of d_{xy}, d_{xz}, and $d_{x^2-y^2}$ functions. The orbital mixing correlates with the absence of any symmetry element. The intricate stereochemistry of **1**−**9** prevents σ/π separation of the interacting orbitals.

As expected, the orbital structure of the lower lying MOs differs remarkably when compared with copper complexes of the [CuN_2S_2] type with saturated ligands (aliphatic thiol-

Table 3. Selected bond lengths [Å], angles, torsion angles [°], and dihedral angles [°] of **1**, **2**, **5**, **6**, **8** (e.s.d.s in parentheses)

Bond lengths [Å]	**1**	**2**	**5**	**6**	**8**[17]
Cu−N(1)	2.001(3)	2.014(6)	1.984(3)	1.994(4)	
Cu−N(2)	2.005(3)	1.986(6)	1.990(3)	2.011(4)	
Cu−S(1)	2.231(1)	2.253(2)	2.217(1)	2.247(2)	
Cu−S(2)	2.262(1)	2.221(2)	2.263(1)	2.219(2)	
N(1)−C(1)	1.319(5)	1.318(8)	1.296(4)	1.295(6)	
C(1)−C(2)	1.429(6)	1.431(9)	1.450(5)	1.454(7)	
C(2)−C(5)	1.402(6)	1.415(9)	1.401(5)	1.398(7)	
C(5)−S(1)	1.716(5)	1.711(7)	1.717(4)	1.718(5)	
C(2)−C(3)	1.438(6)	1.436(9)	1.432(5)	1.417(7)	
C(3)−C(4)	1.512(7)	1.518(9)	1.490(6)	1.500(7)	
C(3)−N(3)	1.311(6)	1.307(9)	1.322(5)	1.322(7)	
N(3)−N(4)	1.383(5)	1.397(7)	1.369(4)	1.373(5)	
N(4)−C(5)	1.425(6)	1.360(8)	1.355(4)	1.354(6)	
N(2)−C(18)	1.312(5)	1.314(9)	1.287(5)	1.303(6)	
C(18)−C(19)	1.425(6)	1.407(9)	1.439(5)	1.445(7)	
C(19)−C(22)	1.418(6)	1.415(9)	1.416(5)	1.405(7)	
C(22)−S(2)	1.721(5)	1.731(8)	1.725(4)	1.718(5)	
C(19)−C(20)	1.429(7)	1.451(9)	1.416(5)	1.444(7)	
C(20)−C(21)	1.497(8)	1.504(9)	1.508(5)	1.512(7)	
C(20)−N(5)	1.317(6)	1.312(9)	1.321(5)	1.302(6)	
N(5)−N(6)	1.381(5)	1.408(8)	1.385(4)	1.372(6)	
N(6)−C(22)	1.346(6)	1.333(9)	1.360(4)	1.358(6)	
N(1)−C(35)	1.425(5)	1.421(9)	1.477(5)	1.469(6)	
N(2)−C(36)	1.418(5)	1.418(9)	1.462(5)	–	
N(2)−C(37)	–	–	–	1.473(6)	
C(35)−C(36)	1.446(6)	1.403(9)	1.506(7)	1.523(8)	
C(36)−C(37)	1.364(6)	1.369(9)	–	1.522(8)	
Angles [°]					
S(1)−Cu(1)−S(2)	88.3(1)	91.5(1)	90.2(1)	87.3(1)	88.1
S(1)−Cu(1)−N(1)	96.2(1)	92.6(2)	98.8 (1)	96.7(1)	99.6
N(1)−Cu(1)−N (2)	81.7(1)	80.7(3)	86.0(1)	91.6(2)	98.1
N(2)−Cu(1)−S(2)	93.7(1)	95.5(2)	96.5(1)	98.5(1)	100.2
S(1)−Cu(1)−N(2)	177.2(1)	168.8(2)	153.8(1)	154.5(1)	
S(2)−Cu(1)−N(1)	174.9(1)	175.6(2)	154.0(1)	147.5(1)	
Cu(1)−S(1)−C(5)	103.2(2)	97.2(2)	104.7(1)	104.1(2)	
Cu(1)−S(2)−C(22)	99.7(2)	102.0(3)	103.4(1)	106.7(2)	
Cu(1)−N(1)−C(1)	128.8(3)	127.7(5)	133.4(2)	131.7(3)	
Cu(1)−N(2)−C(18)	128.6(3)	129.4(6)	130.2(3)	131.8(3)	
Cu(1)−N(1)−C(35)	108.1(1)	124.6(7)	106.3(2)	108.1(3)	
Cu(1)−N(2)−C(36)	107.8(3)	106.5(5)	109.8(2)	–	
N(1)−C(35)−C(36)	114.3(4)	113.0(8)	108.9(3)	110.1(4)	
N(2)−C(36)−C(35)	114.6(3)	116.5(8)	109.0(4)	–	
N(1)−C(1)−C(2)	121.5(4)	119.3(7)	122.1(3)	122.3(4)	
N(2)−C(18)−C(19)	121.8(4)	120.9(7)	124.1(3)	123.6(4)	
C(1)−C(2)−C(5)	127.4(4)	125.9(6)	126.6(3)	126.8(4)	
C(18)−C(19)−C(22)	126.9(4)	127.9(8)	126.5(3)	128.0(4)	
C(2)−C(5)−S(1)	131.5(3)	131.5(6)	133.4(3)	131.3(4)	
C(19)−C(22)−S(2)	129.7(4)	130.6(7)	130.6(3)	131.4(4)	
Cu(1)−N(2)−C(37)	–		–	109.0(3)	
C(35)−C(36)−C(37)	–		–	112.5(5)	
N(2)−C(37)−C(36)	–	–	–	110.1(4)	
Torsion angles [°]					
N(1)−C(35)−C(36)−N(2)	1.6	−1.3	48.5	–	
N(1)−C(35)−C(36)−C(37)	–	–	–	−33.5	
N(2)−C(37)−C(36)−C(35)	–	–	–	−48.8	
Cu(1)−N(1)−C(1)−C(2)	18.3	−15.3	−8.0	1.9	
Cu(1)−N(2)−C(18)−C(19)	−12.7	19.6	7.6	1.5	
N(1)−C(1)−C(2)−C(5)	13.4	−20.1	7.5	18.4	
N(2)−C(18)−C(19)−C(22)	−15.1	11.5	15.6	0.7	
C(1)−C(2)−C(5)−S(1)	−13.6	3.0	2.2	−7.4	
C(18)−C(19)−C(22)−S(2)	−3.0	−7.0	−6.4	−2.6	
C(2)−C(5)−S(1)−Cu(1)	−12.1	34.9	−8.4	−16.0	
C(19)−C(22)−S(2)−Cu(1)	34.4	−19.8	−17.3	1.8	
C(5)−S(1)−Cu(1)−N(1)	27.0	−44.5	5.8	23.1	
C(22)−S(2)−Cu(1)−N(2)	−40.2	31.6	25.8	0.0	
S(1)−Cu(1)−N(1)−C(1)	−36.4	47.1	0.8	−21.7	
S(2)−Cu(1)−N(2)−C(18)	39.8	−39.8	−27.1	−1.6	
Dihedral angles [°]					
θ	3.3	9.0	34.7	42.5	52.1

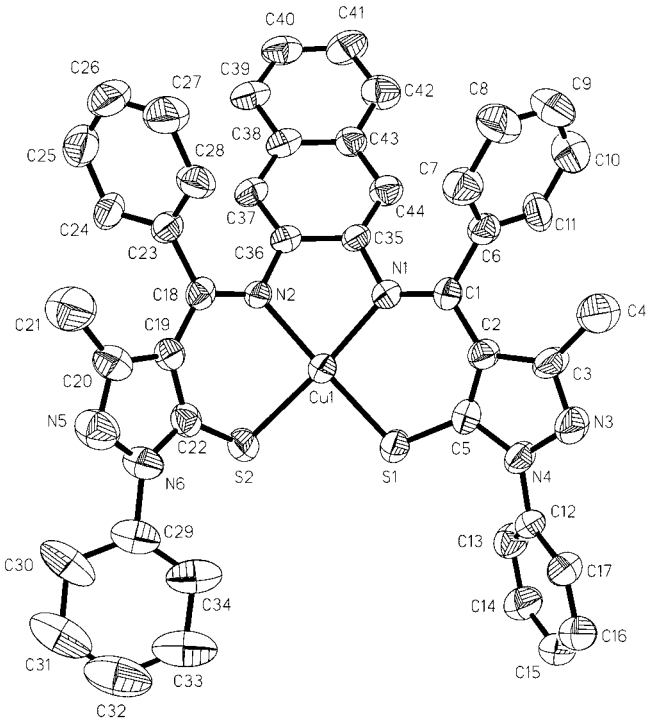

Figure 4. Molecular structure of complex **1** ($\theta = 3.3°$); hydrogen atoms and solvent molecules are omitted for clarity (ORTEP drawing with 50% probability ellipsoids)

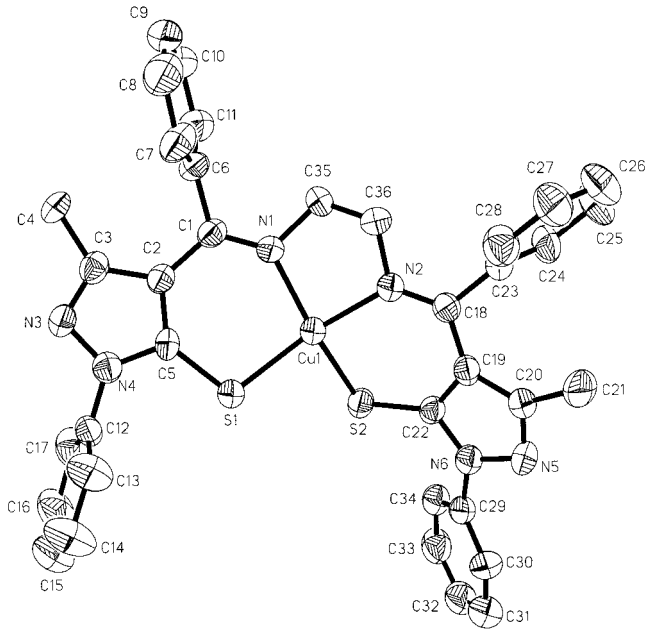

Figure 5. Molecular structure of complex **5** ($\theta = 34.7°$); hydrogen atoms and solvent molecules are omitted for clarity (ORTEP drawing with 50% probability ellipsoids)

ates).[31] In this case, the MOs arranged below the SOMO are typical sulfur lone-pair orbitals, whereas **1**−**9** are distinguished by largely delocalized MOs. The doubly occupied orbitals 6*a* and 5*a* are delocalized over the phenylpyrazole building block of the ligand with a ca. 20% contribution of the sulfur donor atoms. The following four orbitals at lower energies are mainly delocalized within the imine and pyrazole fragment with a more (4*a*, 1*a*) or less (3*a*, 2*a*) strong contribution of the thiolate sulfur. The three lowest unoccupied MOs calculated are mainly localized at the imine and pyrazole fragment.

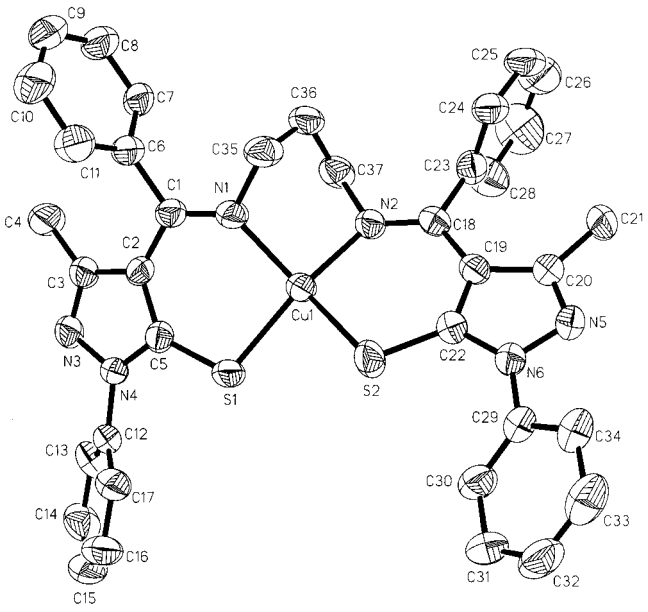

Figure 6. Molecular structure of complex **6** ($\theta = 42.5°$); hydrogen atoms and solvent molecules are omitted for clarity (ORTEP drawing with 50% probability ellipsoids)

The orbital characteristics obtained for the ethylene-bridged ligand system **5** agree with those of **1**, **6** and **8** distinguished by different *N*,*N*′-diamine backbones. Interestingly, the nearly planar complex **1** shows primarily an MO-localized at the imine functions arranged between the S-containing orbitals.

Single vacancy on the copper-containing SOMO and the existence of lower lying sulfur lone-pair orbitals should lead to the appearance of LMCT absorption in the low-energy region of the electronic spectra of the $[CuN_2S_2]$ complexes **1**−**9** (Table 5). Usually, the UV/Vis spectra of these complexes are dominated by three LMCT bands of σ and π symmetry in the range 350−500 nm.[25] In the electronic spectra of the complexes with the pyrazole-based thiolate ligands **1**−**9** two absorption bands in the regions 484−660 nm and 410−530 nm were assigned to transitions from sulfur-containing MOs to the SOMO.[19] A third absorption at shorter wavelength should be superimposed by the long-wavelength side of the intraligand (IL) π-π* absorption bands. Due to the strong delocalization calculated for the S-containing donor orbitals of the electronic transitions, the lowest energy absorption of the complexes **1**−**9** should possess π-π* character.

Increasing tetrahedral distortion of $[CuN_2S_2]$ complexes leads to red-shifted absorption in the UV/Vis spectra.[10][32] EHMO calculations confirm these experimental findings. With an increasing dihedral angle θ between the planes N_1CuS_1 and N_2CuS_2, the energy of the SOMO (its antibonding nature is the largest in the planar arrangement) is

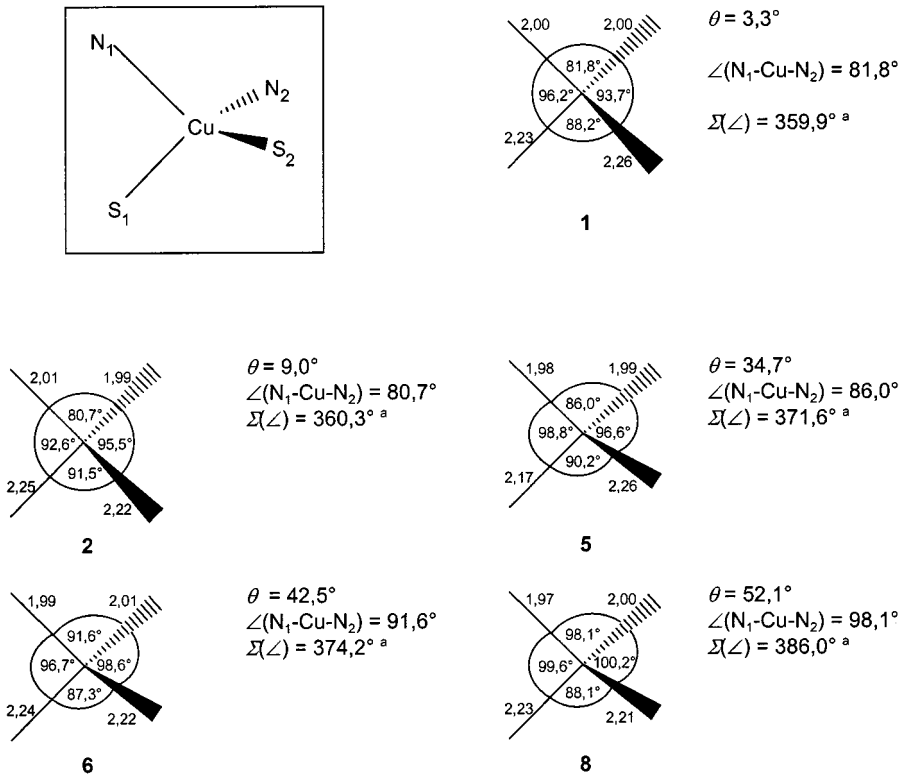

Figure 7. Comparison of the geometrical changes in the coordination polyhedra **1**, **2**, **5**, **6**, and **8** and enlargement of the N_1-Cu-N_2 bite angle dependent on the bridging diamine unit **R** [$\Sigma(\angle) = 360°$ ideal planar arrangement, $\Sigma(\angle) = 437.6°$ ideal tetrahedral arrangement of all donor atoms around the central ion Cu^{2+}]

Table 4. UV/Vis-spectroscopic data of the ligands H_2**1**$-H_2$**9**

Ligand	Backbone **R**	λ_{max} (ε) [nm (in L mol^{-1} cm^{-1})] {293 K; $CHCl_3$}
H_2**1**	2,3-naphthyl	271 (37300), 321 (34000), 419 (11700)
H_2**2**	1,2-phenyl	276 (35500), 318 (35800), 421 (11900)
H_2**3**	4-methylphenyl	275 (34800), 317 (35100), 419 (12300)
H_2**4**	3,4-dichlorophenyl	271 (36000), 321 (36000), 426 (10900)
H_2**5**	$-CH_2-CH_2-$	277 (26100), 314 (31200), 399 (11700)
H_2**6**	$-CH_2-CH_2-CH_2-$	281 (24500), 310 (29900), 394 (11100)
H_2**7**	$-CH_2-C(CH_3)_2-CH_2-$	282 (25600), 311 (31200), 394 (11400)
H_2**8**	2,2′-biphenyl	271 (32800), 321 (26300), 419 (10600)
H_2**9**	2,2′-binaphthyl	284 (37900), 344 (28300), 446 (12100)

successively decreased with increasing θ, whereas the energies of the doubly occupied S-containing MOs and the lowest unoccupied MOs remain nearly constant. In order to make the energetical changes in the frontier orbital region more obvious and to simplify the MO analysis by excluding the backbones between the two imine nitrogen atoms a purposely idealized C_{2v} model system **A** with planar NC_3S groups has been considered (Figure 9). Fixed averaged bond lengths and angles obtained from the structural data of complexes **1**, **5**, and **6** have been used as idealized geometrical parameters of the NS ligands. The hydrogen atoms were calculated in ideal positions.

The results of EHT calculations clearly show the overlap between d functions and ligand orbitals of appropriate symmetry to be most effective for $\theta = 0$. One ligand of the model fragment was fixed and the other ligand was stepwise rotated around the bisector of the N_1-Cu-S_1 angle simulating an increasing θ. This method has limitations in fitting to the actual structures that are in contrast to the actual molecules, the S_1-Cu-S_2 bite angles are successively increased in the model fragment with increasing θ. Regardless of this limitation, the more the ligand field is distorted (pointgroup changes from C_{2v} for $\theta = 0$ to C_2 for $\theta > 0$), the more the SOMO is stabilized (Figure 10). The SOMO ($2b_2$ for $\theta = 0$ or $3b$ for $\theta > 0$) is an antibonding orbital constructed with σ-type lone-pair orbitals from the four donor atoms and the copper d_{xy} AO. A considerable admixture of Cu p functions to $3b$ is observed for the nonplanar C_2 systems.

The highest fully occupied MO ($1a_2$ for $\theta = 0$, $2a$ for $\theta > 0$) is vice versa destabilized with increasing θ, but no orbital crossing occurs between SOMO $3b$ and the fully occupied orbital $2a$ for $0 \leq \theta \leq 90°$. The unoccupied π* MOs $3a$ and $4b$ and the π MO $2b$ are nearly unaffected by the

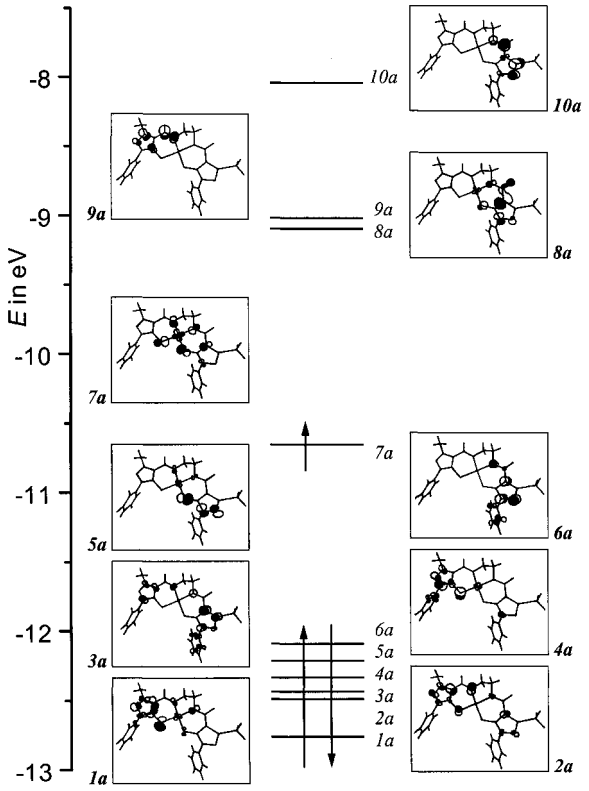

Figure 8. MO diagram of the model complex derived from **5**

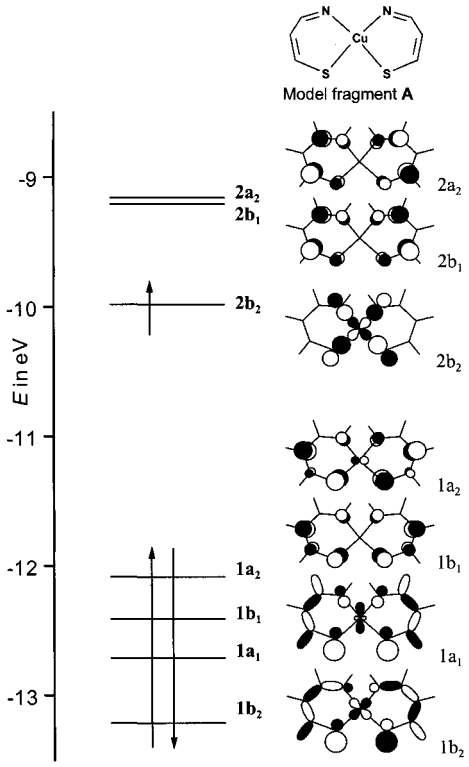

Figure 9. MO diagram of the C_{2v} model fragment **A**

Table 5. UV/Vis-spectroscopic data of the complexes **1**−**9**

Complex	Backbone **R**	λ_{max} (ε) [L mol^{-1} cm^{-1}] {293 K; $CHCl_3$}
1	2,3-naphthyl	484 (sh) (4300), 410 (sh) (16200), 336 (41600), 275 (41400)
2	1,2-phenyl	500 (sh) (2500), 405 (sh) (11900), 344 (32900), 275 (37500)
3	(4-methyl)phenyl	500 (sh) (2500), 410 (sh) (12200), 345 (33600), 277 (39400)
4	(3,4-dichloro)phenyl	505 (sh) (2500), 410 (sh) (14100), 350 (33700), 317 (28400), 279 (34000)
5	$-CH_2-CH_2-$	520 (sh) (1600), 438 (3500), 346 (sh) (10800), 275 (35600)
6	$-CH_2-CH_2-CH_2-$	610 (sh) (1900), 476 (3900), 339 (12100), 274 (36700)
7	$-CH_2-C(CH_3)_2-CH_2-$	599 (1900), 473 (3700), 341 (11500), 272 (35500)
8	2,2′-biphenyl	630 (sh) (1400), 522 (2100), 350 (sh) (10800), 279 (35500)
9	2,2′-binaphthyl	659 (1600), 530 (1800), 355 (sh) (17000), 290 (51800)

geometrical changes, and the levels 1*b* and 1*a* display only minor shifts. Generally it is hard to detect any further trends for these levels and for the interpretation of the electronic spectra of complexes **1**−**9**, because of the orbital mixing of all close-lying orbitals of the same symmetry type (*a* or *b*).

The results of the EHMO calculations are also in good agreement with the EPR data for complexes **1**−**9**. All complexes considered display typical Cu^{II} EPR signals with the four copper lines showing additional hyperfine splitting due to the coordination of two nitrogen donors (Table 6). The a_0^{Cu} values for **1**−**4** are as expected for planar Cu^{II} chromophores ($79-80\times10^{-4}$ cm^{-1}), while **5** shows a decreased a_0^{Cu} value due to a noticeable tetrahedral distortion. With a stronger deviation from the planar donor arrangement, the a_0^{Cu} values decline considerably, with the lowest value being obtained for **9**.

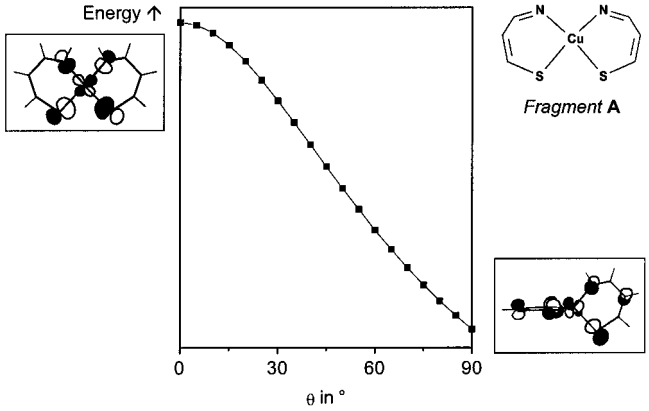

Figure 10. SOMO energy of the model fragment **A** in correlation to the dihedral angle θ

Table 6. EPR[a] (g_0, a_0^{Cu} at 293 K; $g_\parallel$, $g_\perp$, $A_\parallel^{Cu}$, $A_\perp^{Cu}$ at 130 K) and electrochemical data[b] of the complexes **1**−**9**

Complex	293 K g_0	a_0^{Cu} [10^{-4} cm^{-1}]	$g_\parallel$	$g_\perp$	130 K $A_\parallel^{Cu}$ [10^{-4} cm^{-1}]	$A_\perp^{Cu}$ [10^{-4} cm^{-1}]	Redox potentials[13] vs. Fc/Fc$^+$ $E_{p,c}$(red) [V]	$E_{p,a}$(ox) [V]
1	2.069	80.20	2.173	2.038	160	26	−1.03[d]	0.31[d]
2	2.070	80.32	2.135	2.037	173	36	−1.04[d]	0.34[d]
3	2.069	80.20	2.175	2.039	162	30	−1.06[d]	0.32[d]
4	2.069	79.45	2.152	2.027	194	25	−0.94[d]	0.42[d]
5	2.066	77.66	2.128	2.035	169	34	−1.23[c]	0.27[c]
6	2.070	69.32	2.137	2.034	161	26	−1.04[c]	0.23[d]
7	2.070	67.04	2.137	2.033	150	25	−1.02[c]	0.24[d]
8	2.072	68.19	2.147	2.035	148	28	−0.89[c]	0.25[d]
9	2.065	66.60	2.132	2.031	141	29	−0.84[c]	0.29[d]

[a] In $CHCl_3$. − [b] In butyronitrile at 293 K. − [c] Electrochemically reversible. − [d] Electrochemically irreversible

Because of the relatively low g values, the copper d orbital contribution to the SOMO of **1**−**9** was estimated from the EPR data.[33] The results obtained are comparable with data from MO calculations yielding a copper contribution to the SOMO of approximately 30−40%. The overall copper contribution on this orbital splits between the p and d functions and remains unaffected by the tetrahedral twist, but the more distorted systems show weaker contributions of the d functions to the SOMO. This finding points to an increased covalency in the tetrahedrally more distorted complexes.

The stepwise decrease of the energy of the SOMO with an increasing dihedral angle θ also influences the redox potentials of compounds **1**−**9**. A detailed description of this electrochemical behaviour of **1**−**9** is given elsewhere,[13] but the trend is that the higher the degree of distortion, the easier the compound can be reduced (Table 6). However, the positive shift of the reduction potentials with increasing tetrahedral distortion within the complex series can only be found after separating the aromatic bridged complexes **1**−**4**, **8**, and **9** from the aliphatic bridged compounds **5**−**7**. This result shows the limits of EHMO calculations in predicting the electrochemical behavior of the considered complexes. The oxidation potentials of **1**−**9** seem to be independent of the coordination geometry. In correlation to the calculated orbitals, the nature of the orbital where the electron is removed from is obviously similar for all considered complexes.

Conclusions

The tetrahedral distortion of the donor sphere in the considered complexes can be influenced by the choice of diamines used for the preparation of the Schiff base ligands. The stereochemistry observed for the different complexes is mainly a result of the interaction between the steric requirements introduced by the ligands and the increasing stabilizing bonding interactions (SOMO) which occur when the ligand field is distorted from planarity. The MO studies of these complexes are complicated by the orbital mixing correlating with the absence of any symmetry elements. The presented results confirm that the unpaired electron is localized in an antibonding orbital formed by σ-type lone pairs of the ligand and a mixed copper p and d contribution. The energy of the SOMO drops and the Cu p contribution increases with larger tetrahedral distortion of the [CuN_2S_2] group. These effects are reflected in bathochromically shifted CT absorptions in the UV/Vis spectra and positively shifted reduction potentials. The increased covalence nature in the tetrahedrally distorted complexes is manifested in declining coupling constants a_0^{Cu} in the EPR spectra of the studied complexes.

Experimental Section

General: Analytical-grade chemicals were used as received from Fluka (several diamines), Laborchemie Apolda [$Cu(CH_3COO)_2$-H_2O] and Merck (solvents for spectroscopy). Elemental analysis were carried out with a Heraeus CHN-O-RAPID analysator. NMR spectra were recorded with a 400-MHz spectrometer (Unity 400, Varian) at room temperature in $CDCl_3$. Electronic spectra were measured with a CARY 3 UV/Vis spectrometer (Varian). An ESP 300E (Bruker) spectrometer (X-band 9.8 GHz) was used to record the ESR spectra at 293 K and at 130 K. − The Schiff base ligands H_2**5**, H_2**6**, and H_2**8** were synthesized according to a literature procedure.[18] This method was extended to prepare the new ligands H_2**1**−H_2**4**, H_2**7**, and H_2**9**.

Schiff Base $H_2$1: M.p. 267°C. − ^{1}H NMR ($CDCl_3$): δ = 7.21−7.83 (m, aromatic H), 1.58 (s, −CH_3), 16.10 (s, >N−H···). − ^{13}C NMR ($CDCl_3$): δ = 15.62 (s, −CH_3), 151.65 (s, >C=N−N), 113.46 (s, >C=), 168.95 (s, >C=S), 166.29 (s, >C=N), 125.50−139.25 (m, aromatic C). − $C_{44}H_{34}N_6S_2$ (710.9): calcd. C 74.34, H 4.82, N 11.82, S 9.02; found C 73.4, H 4.9, N 11.3, S 9.1.

Schiff Base $H_2$2: M.p. 259−261°C. − ^{1}H NMR ($CDCl_3$): δ = 6.75−7.85 (m, aromatic H), 1.56 (s, −CH_3), 15.98 (s, >N−H···). − ^{13}C NMR ($CDCl_3$): δ = 16.06 (s, −CH_3), 152.05 (s, >C=N−N), 113.71 (s, >C=), 169.53 (s, >C=S), 166.64 (s, >C=N), 125.96−139.66 (m, aromatic C). − $C_{40}H_{32}N_6S_2$ (660.9): calcd. C 72.70, H 4.88, N 12.72, S 9.70; found C 73.0, H 4.9, N 12.6, S 9.34.

Schiff Base $H_2$3: M.p. 248−249°C. − ^{1}H NMR ($CDCl_3$): δ = 6.55−7.85 (m, aromatic H), 1.54 (s, −CH_3), 1.56 (s, −CH_3), 15.88 (s, >N−H···), 2.01 (s, −CH_3). − ^{13}C NMR ($CDCl_3$): δ = 16.05 (s, −CH_3), 16.01 (s, −CH_3), 152.09 (s, >C=N−N), 112.80 (s, >C=), 113.63 (s, >C=), 169.12 (s, >C=S), 166.79 (s, >C=N); 166.73 (s, >C=N), 125.96−139.18 (m, aromatic C), 21.27 (s, −CH_3). −

$C_{41}H_{34}N_6S_2$ (674.9): calcd. C 72.97, H 5.08, N 12.45, S 9.50; found C 72.7, H 5.0, N 12.4, S 9.4.

Schiff Base $H_2$4: M.p. 271−273°C. − ^{1}H NMR ($CDCl_3$): δ = 6.76−7.83 (m, aromatic H), 1.56 (s, $-CH_3$), 15.68 (s, >N−H···). − ^{13}C NMR ($CDCl_3$): δ = 16.10 (s, $-CH_3$), 152.10 (s, >C=N−N), 114.06 (s, >C=), 170.01 (s, >C=S), 165.78 (s, >C=N), 125.83−139.30 (m, aromatic C). − $C_{40}H_{30}Cl_2N_6S_2$ (729.8): calcd. C 65.83, H 4.14, Cl 9.72, N 11.52, S 8.79; found C 65.6, H 4.5, Cl 10.2, N 11.5, S 8.9.

Schiff Base $H_2$5: M.p. 284−286°C. − ^{1}H NMR ($CDCl_3$): δ = 7.16−7.76 (m, aromatic H), 1.37 (s, $-CH_3$), 14.54 (s, >N−H···), 3.50 (m, $-CH_2-$). − ^{13}C NMR ($CDCl_3$): δ = 15.28 (s, $-CH_3$), 151.49 (s, >C=N−N), 112.29 (s, >C=), 169.03 (s, >C=S), 167.79 (s, >C=N), 125.39−139.55 (m, aromatic C), 44.80 (s, $-CH_2-$). − $C_{36}H_{32}N_6S_2$ (612.8): calcd. C 70.56, H 5.26, N 13.71, S 10.46; found C 70.0, H 5.4, N 13.5, S 10.8.

Schiff Base $H_2$6: M.p. 212−214°C. − ^{1}H NMR ($CDCl_3$): δ = 7.30−7.80 (m, aromatic H), 1.35 (s, $-CH_3$), 14.37 (s, >N−H···), 3.39 (m, $-CH_2-$N), 1.92 (m, C$-CH_2-$C). − ^{13}C NMR ($CDCl_3$): δ = 15.30 (s, $-CH_3$), 151.74 (s, >C=N−N), 112.19 (s, >C=), 169.66 (s, >C=S), 167.78 (s, >C=N), 126.24−140.85 (m, aromatic C), 43.36 (s, $-CH_2-$N=), 30.05 ($-CH_2-$). − $C_{37}H_{34}N_6S_2$ (626.9): calcd. C 70.89, H 5.47, N 13.41, S 10.23; found C 71.0, H 5.4, N 13.4, S 10.8.

Schiff Base $H_2$7: M.p. 206−208°C. − ^{1}H NMR ($CDCl_3$): δ = 7.22−7.84 (m, aromatic H), 1.41 (s, $-CH_3$), 14.41 (s, >N−H···), 3.30 (m, $-CH_2-$), 1.18(s, $-CH_3$). − ^{13}C NMR ($CDCl_3$): δ = 15.25 (s, $-CH_3$), 151.40 (s, >C=N−N), 112.32 (s, >C=), 168.89 (s, >C=S), 167.05 (s, >C=N), 125.87−139.35 (s, arom. C), 36.08 (s, >C<), 54.13 (s, $-CH_2$), 24.54 (s, $-CH_3-$). − $C_{39}H_{38}N_6S_2$ (654.9): calcd. C 71.53, H 5.85, N 12.83, S 9.79; found C 71.4, H 5.5, N 11.7, S 9.9.

Schiff Base $H_2$8: M.p. 214−217°C. − ^{1}H NMR ($CDCl_3$): δ = 6.75−7.85 (m, aromatic H), 1.45 (s, $-CH_3$), 15.53 (s, >NH···). − ^{13}C NMR ($CDCl_3$): δ = 16.01 (s, $-CH_3$), 151.62 (s, >C=N−N), 114.05 (s, >C=), 170.03 (s, >C=S), 166.87 (s, >C=N), 125.86...139.48 (m, arom. C). − $C_{46}H_{36}N_6S_2$ (737.0): calcd. C 74.98, H 4.92, N 11.40, S 8.70; found C 74.2, H 5.4, N 11.8, S 8.3.

Schiff Base $H_2$9: M.p. 310−315°C. − ^{1}H NMR ($CDCl_3$): δ = 6.70−7.79 (m, aromatic H), 1.44 (s, $-CH_3$), 15.65 (s, >N−H···). − ^{13}C NMR ($CDCl_3$): δ = 16.38 (s, $-CH_3$), 151.32 (s, >C=N−N), 133.49 (s, >C=), 169.08 (s, >C=S), 163.90 (s, >C=N), 125.25−139.62 (m, aromatic C). − $C_{54}H_{40}N_6S_2$ (837.1): calcd. C 77.48, H 4.82, N 10.04, S 7.66; found C 76.1, H 5.2, N 9.3, S 7.8.

Complexes **1−9** were synthesized with the appropriate ligands and $Cu(CH_3COO)_2{\cdot}H_2O$ in ethanol according to a literature procedure.[17]

Cu Complex 1: M.p. 338°C. − $C_{44}H_{32}CuN_6S_2$ (772.5): calcd. C 68.41, H 4.18, Cu 8.23, N 10.88, S 8.30; found C 67.8, H 4.0, Cu 8.8, N 10.5, S 7.9.

Cu Complex 2: M.p. 329−331°C. − $C_{40}H_{30}CuN_6S_2$ (722.4): calcd. C 66.51, H 4.19, Cu 8.80, N 11.62, S 8.88; found C 66.7, H 4.3, Cu 8.7, N 11.8, S 8.6.

Cu Complex 3: M.p. 302°C. − $C_{41}H_{32}CuN_6S_2{\cdot}CHCl_3$(855.8): calcd. C 58.95, H 3.88, Cl 12.43, Cu 7.42, N 9.83, S 7.49; found C 58.7, H 3.7, Cl 12.6, Cu 6.9, N 9.7, S 8.2.

Cu Complex 4: M.p. 333−336°C. − $C_{40}H_{28}Cl_2CuN_6S_2$ (791.3): calcd. C 60.71, H 3.57, Cl 8.96, Cu 8.04, N 10.62, S 8.10; found C 60.7, H 3.8, Cl 8.7, Cu 9.5, N 10.8, S 8.1.

Cu Complex 5: M.p. 324−326°C. − $C_{36}H_{30}CuN_6S_2$ (674.3): calcd. C 64.12, H 4.48, Cu 9.42, N 12.46, S 9.52; found C 63.9, H 4.8, Cu 9.1, N 12.5, S 10.0.

Cu Complex 6: M.p. 282−285°C. − $C_{37}H_{32}CuN_6S_2$ (688.4): calcd. C 64.56, H 4.69, Cu 9.23, N 12.21, S 9.31; found C 64.2, H 5.1, Cu 9.6, N 12.1, S 8.2.

Cu Complex 7: M.p. 262°C. − $C_{39}H_{36}CuN_6S_2$ (716.4): calcd. C 65.39, H 5.06, Cu 8.87, N 11.73, S 8.95; found C 64.2, H 5.1, Cu 9.6, N 12.1, S 8.2.

Cu Complex 8: M.p. > 306°C (decomp.). − $C_{46}H_{34}CuN_6S_2$ (798.5): calcd. C 69.19, H 4.29, Cu 7.97, N 10.52, S 8.03; found C 68.7, H 4.4, Cu 7.7, N 10.4, S 7.7.

Cu Complex 9: M.p. 346°C (decomp.). − $C_{54}H_{38}CuN_6S_2$ (898.6): calcd. C 72.18, H 4.26, Cu 7.07, N 9.35, S 7.14; found C 71.6, H 4.3, Cu 8.0, N 9.3, S 7.9.

X-ray Crystal-Structure Determination: Detailed structure data for H_2**5**, **1**, **2**, **5**, and **6** can be obtained from the Cambridge Crystallographic Data Centre. The deposition numbers are CCDC-101708 (H_2**5**), -101711 (**1**), -101712 (**2**), -101710 (**5**), and -101713 (**6**). Suitable crystals were obtained by diffusion of *n*-decane or *n*-hexane into saturated solutions of **1**, **2** and **6** in $CHCl_3$. Crystals of **5** precipitated during slow concentration of a saturated ethanolic solution at −20°C, single crystals of H_2**5** precipitated from an EtOH/$CHCl_3$ mixture. Crystallographic data for H_2**5**, **1**, **2**, **5**, and **6** are listed in Table 1. Selected bond lengths and angles are given in Tables 2 and 3. Figures 2−6 display thermal-ellipsoid drawings of 50% probability. Crystals were mounted on a glass pin. Data were collected at room temperature with a Siemens CCD diffractometer (SMART) operating in the ω-scan mode (**1**, **5**, **6**) or a Stoe four-circle diffractometer (STADI 4) operating in the ω/2θ-scan mode (**2**). Data for H_2**5** were collected with a Nonius CCD diffractometer. All diffractometers were equipped with a monochromator utilizing Mo-K_α radiation (λ = 0.7107 Å). Empirical absorption correction (SADABS[34]) was applied for **1**, **5**, and **6.** A ψ-scan correction was used for **2.** All observed reflections of H_2**5**, **1**, **5**, and **6** were used for refinement of unit-cell parameters. 80 reflections with 20° < Θ < 25° were selected for complex **2**. All structures were solved using direct methods (SHELXS[35]). Parameters were refined by full-matrix least-squares techniques (SHELXL[36]). Partly, the hydrogen atoms were calculated in ideal positions and their isotropic thermal parameters were fixed. For **5**, the water hydrogen atoms could not be localized in the structure.

Calculational Methods: The Extended Hückel LCAO Calculations[37] were carried out using methods as proposed by Mealli.[38] Considering the calculation of transition metal complexes, the weighted H_{ij} formula (modified Wolfberg-Helmholtz relation) for the off-diagonal elements (H_{ij}) was used, to take into consideration the counterintuitive orbital mixing.[39] Single Slater-type orbitals were used for the main-group elements as well as for the s and p functions of the metal ion, whereas d wave functions were taken as contracted linear combinations of two Slater-type functions as proposed by Richardson.[40] The crystallographic data (atomic coordinates) of the complexes **1**, **2**, **5**, **6**, and **8** (Cambridge Crystallographic Data Centre) were taken for the calculations to fit the molecular geometry. In all cases the phenyl rings on C(1) and C(18) were replaced by hydrogen atoms calculated in ideal positions. Atomic coordinates for dimethyl *N*,*N*′-ethylenebis(L-cysteinato)-*S*,*S*′]copper(II) were included for comparison (Cambridge Crystallographic Data Centre).

Acknowledgments

This work was supported by the Deutsche Forschungsgemeinschaft and the Fonds der Chemischen Industrie. We thank Prof. R. Kirmse and A. Voigt (University of Leipzig) for the EPR investigations.

[1] S. Otsuka, T. Yamanaka, *Metalloproteins − Chemical and Biological Effects*, *Bioactive Molecules*, Elsevier Science Publ., Amsterdam, **1988**, vol. 8.
[2] T. G. Spiro (Ed.), *Copper Proteins*, Wiley & Sons, New York, **1981**.
[3] K. D. Karlin, Y. Gultneh, *Prog. Inorg. Chem.*, **1987**, *35*, 219.
[4] A. Messerschmidt, *Adv. Inorg. Chem*. **1993**, *40*, 121.
[5] W. Kaim, J. Rall, *Angew. Chem.* **1996**, *108,* 47.
[6] P. M. Colman, H. C. Freeman, J. M. Guss, M. Murata, V. A. Norris, J. A. M. Ramshaw, M. P. Venkatappa, *Nature*, **1978**, *160*, 309.
[7] E. T. Adman, R. E. Stenkamp, L. C. Sieker, L. H. Jensen, *J. Mol. Biol.* **1978**, *123*, 35.
[8] A. G. Sykes, *Adv. Inorg. Chem.* **1991**, *36*, 377.
[9] B. P. Murphy, *Coord. Chem. Rev.* **1990**, *124*, 63.
[10] E. I. Solomon, M. J. Baldwin, M. D. Lowery, *Chem. Rev.* **1992**, *92*, 521.
[11] N. Kitajima, Adv. *Inorg. Chem.* **1993**, *39*, 1.
[12] T. Tsukihara, H. Aoyama, E. Yamashita, T. Tomizaki, H. Yamaguchi, K. Shinzawa-Itoh, R. Nakashima, R. Yaono, S. Yoshikawa, *Science* **1995**, *269*, 1069.
[13] S. Knoblauch, F. Hartl, D. J. Stufkens, H. Hennig, *Eur. J. Inorg. Chem.* **1999**, 303.
[14] H. Hennig, S. Knoblauch, D. Scholz, *New J. Chem.* **1997**, *21*, 701.
[15] M. Grosche, Dissertation, Universität Leipzig, **1993**.
[16] J. Behling, Dissertation, Universität Leipzig, **1994**.
[17] L. Hennig, R. Kirmse, O. Hammerich, S. Larsen, H. Frydendahl, H. Toftlund, J. Becher, *Inorg. Chim. Acta* **1995**, *234*, 67.
[18] L. Hennig, G. Mann, *Z. Chem.* **1988**, *28*, 364.
[19] S. Mandal, G. Das, R. Singh, R. Shukla, P. K. Bharadwaj, *Coord. Chem. Rev.* **1997**, *160,* 191.
[20] E. I. Solomon, K. W. Penfield, D. E. Wilcox, *Struct. Bonding* **1983**, *53*, 1.
[21] A. G. Sykes, *Struct. Bonding* **1990**, *75*, 175.
[22] H. B. Gray, E. I. Solomon, in *Copper proteins* (Ed.: T.G. Spiro), Wiley & Sons, New York, **1981**.
[23] A. Messerschmidt, *Struct. Bonding* **1998**, *90*, 37.
[24] H. Toftlund, J. Becher, P. H. Olesen, J. Z. Pedersen, *Israel J. Chem.* **1985**, *25*, 56.
[25] H. J. Schugar, *Copper Coordination Chemistry*, Adenine Press, New York, **1984**, p. 43.
[26] S. Mandal, R. Shukla, P. K. Bharadwaj, *Polyhedron* **1995**, *14*, 2063.
[27] M. Gullotti, L. Casella, A. Pintar, E. Suardi, P. Zanello, S. Mangani, *J. Chem. Soc., Dalton Trans.* **1989**, 1979.
[28] R. D. Bereman, M. R. Churchill, G. Shields, *Inorg. Chem.* **1979**, *18*, 3117.
[29] T. Yamabe, K. Hori, T. Minato, K. Fukui, Y. Sugiura, *Inorg. Chem.* **1982**, *21*, 2040.
[30] R. Cini, A. Cinquantini, P. L. Orioli, C. Mealli, M. Sabat, *Can. J. Chem.* **1984**, *62*, 2908−2913.
[31] P. K. Bharadwaj, J. A. Potenza, H. J. Schugar, *J. Am.Chem. Soc.* **1986**, *108*, 1351.
[32] R. L. Harlow, W. J. Wells, G. W. Watt, S. H. Simonsen, *Inorg. Chem.* **1975**, *14*, 1768.
[33] J. R. Morton, K. F. Preston, *J. Magn. Reson.* **1978**, *30*, 577.
[34] R. H. Blessing, *Acta Crystallogr.* **1995**, *51A*, 33.
[35] G. M. Sheldrick, *SHELXS-86*, Universität Göttingen, **1986**.
[36] G. M. Sheldrick, *SHELXL-97*, Universität Göttingen, **1997**.
[37] R. Hoffmann, *Chem. Phys.* **1963**, *39*, 1397.
[38] C. Mealli, D. M. Prosperio, *J. Chem. Educ.* **1990**, *76*, 399.
[39] J. H. Ammeter, H. B. Bürgi, J. C. Thibeault, R. Hoffmann, *J. Am. Chem. Soc.* **1978**, *100*, 3686.
[40] J. W. Richardson, W. C. Nieuwpoort, R. Powell, W. F. Edgel, *J. Chem. Phys.* **1962**, *36*, 1057.

Received August 12, 1998
[I98274]